

Unit Disk Representations of Embedded Trees, Outerplanar and Multi-Legged Graphs

Sujoy Bhore¹[0000–0003–0104–1659], Maarten Löffler², Soeren Nickel³[0000–0001–5161–3841], and Martin Nöllenburg³[0000–0003–0454–3937]

¹ Indian Institute of Science Education and Research, Bhopal, India
sujoy.bhore@gmail.com

² Department of Computing and Information Sciences, Utrecht University
m.loffler@uu.nl

³ Algorithms and Complexity Group, TU Wien, Vienna, Austria
[soeren.nickel|noellenburg]@ac.tuwien.ac.at

Abstract. A unit disk intersection representation (UDR) of a graph G represents each vertex of G as a unit disk in the plane, such that two disks intersect if and only if their vertices are adjacent in G . A UDR with interior-disjoint disks is called a unit disk contact representation (UDC). We prove that it is NP-hard to decide if an outerplanar graph or an embedded tree admits a UDR. We further provide a linear-time decidable characterization of caterpillar graphs that admit a UDR. Finally we show that it can be decided in linear time if a lobster graph admits a *weak* UDC, which permits intersections between disks of non-adjacent vertices.

1 Introduction

The representation of graphs as contacts or intersections of disks has been a major topic of investigation in geometric graph theory and graph drawing. The famous circle packing theorem states that every planar graph has a contact representation by touching disks (of various size) and vice versa [13]. Since then, a large body of research has been devoted to the representation of planar graphs as contacts or intersections of various kinds of geometric objects [4,5,8,9]. In this paper, we are interested in unit-radius disks. A set of unit disks in \mathbb{R}^2 is a *unit disk intersection representation* (UDR) of a graph $G = (V, E)$, if there is a bijection between V and the set of unit disks such that two disks intersect if and only if they are adjacent in G . *Unit disk graphs* are graphs that admit a UDR. *Unit disk contact graphs* (also known as *penny graphs*) are the subfamily of unit disk graphs that have a UDR with interior-disjoint disks, which is thus called a *unit disk contact representation* (UDC). This can be relaxed to *weak* UDCs, which permit contact between non-adjacent disks; see Fig. 1 for examples.

The recognition problem, where the objective is to decide whether a given graph admits a UDR, has a rich history [1,2,10,11]. Breu and Kirkpatrick [3] proved that it is NP-hard to decide whether a graph G admits a UDR or a UDC, even for planar graphs. Klemz et al. [12] showed that recognizing outerplanar

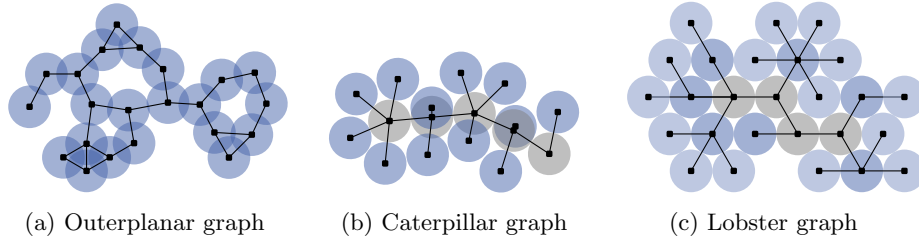


Fig. 1: We investigate specific contact and intersection graphs of unit disks. In a UDR (a-b) disks are allowed to overlap, and contact of two disks implies an edge between their vertices. In a weak UDC the disks are interior disjoint, but contact between non-adjacent disks is allowed. The disks of backbone vertices are colored grey (b-c).

unit disk contact graphs is already NP-hard, but it is decidable in linear time for caterpillars, i.e., trees whose internal vertices form a path (see Fig. 1b).

Recognition with a fixed embedding is an important variant of the recognition problem. Given a plane graph G , the objective in this problem is to decide whether G admits a UDC in the plane that preserves the cyclic order of the neighbors at each vertex. Some recent works investigated the recognition problem of UDCs with/without fixed embedding, and narrowed down the precise boundary between hardness and tractability; see [1,6,7,12]. A remaining open question is to settle the complexity of recognizing non-embedded trees that admit a UDC. Some of these works focused on *weak* UDCs, where disks of non-adjacent vertices may touch. In this model, the recognition of non-embedded trees that admit a weak UDC is NP-hard [7]. We summarize the results on weak UDCs in Table 1.

While several results of the past years have shed light into the recognition complexity gap for UDCs, not much is known in this regard for the more general class of UDRs since the NP-hardness for planar graphs from 1998 [3].

Our Contribution. We investigate the unit disk graph recognition problem for subclasses of planar graphs. We show that recognizing unit disk graphs remains NP-hard for non-embedded outerplanar graphs (see Fig. 1a) – strengthening the previous hardness result for planar graphs [3] – and for embedded trees (Section 3). This line of research aims to extend earlier investigations [1,6,7] of UDCs to the UDR model and builds in particular on the work of Bowen et al. [1].

On the positive side, we provide a linear-time algorithm to recognize caterpillar graphs (see Fig. 1b) that admit a UDR (Section 4). In Section 5, we return to the problem of recognizing unit disk contact graphs and extend the tractability boundary for non-embedded graphs. While it was known that a weak UDC for caterpillar graphs can be constructed in linear time (if one exists), but the same recognition problem is NP-hard for trees [7], we prove that we can decide in linear time if a lobster graph admits a weak UDC on the triangular grid, where a *lobster* is a tree whose internal vertices form a caterpillar (see Fig. 1c). Ta-

graph class	weak UDC		UDR	
	non-embedded	embedded	non-embedded	embedded
planar	\uparrow NP-hard	\uparrow NP-hard	NP-hard [3]	\uparrow NP-hard
outerplanar	\uparrow NP-hard	\uparrow NP-hard	NP-hard (Thm.1)	\uparrow NP-hard
trees	NP-hard [7]	\uparrow NP-hard	open	NP-hard (Thm.2)
lobsters	$O(n)$ (Thm.4)	\uparrow NP-hard	open	open
caterpillars	$O(n)$ [7]	NP-hard [6]	$O(n)$ (Thm.3)	open

Table 1: State of the art, our results, and open problems on unit disk graph recognition. Upward arrows indicate, that a result follows from the one below.

ble 1 summarizes our results and remaining open problems. Proofs and details of results marked with a star (\star) can be found in the appendix.

2 Preliminaries

A graph $G = (V, E)$ with $V = \{v_1, \dots, v_n\}$ is a unit disk graph if there exists a set of closed unit disks $\mathcal{D} = \{d_1, \dots, d_n\}$ and a bijective mapping $d: V \rightarrow \mathcal{D}$, s.t., $d(v_i) = d_i$ and $v_i v_j \in E$ if and only if d_i and d_j intersect. We call \mathcal{D} a *unit disk intersection representation* (UDR) of G . If all disks in \mathcal{D} are pairwise interior disjoint we also call \mathcal{D} a *unit disk contact representation* (UDC) of G . A graph is a *unit disk contact graph* if it admits a UDC. A *weak* UDC permits contact between two disks d_i and d_j , even if $v_i v_j \notin E$.⁴ A *caterpillar* graph G is a tree, which yields a path, when all leaves are removed. We call this path, the backbone B_G of G . Similarly a *lobster* graph G' is a tree, which yields a caterpillar graph G'' , when all leaves are removed. The backbone of G' is the backbone of G'' . For each vertex v of the backbone, we denote the set of vertices that are reachable from v on a path that does not include any other backbone vertex, as the *descendants* of v .

The set of disks \mathcal{D} induces an embedding $\mathcal{E}_{\mathcal{D}}(G)$ of G by placing every vertex v at the center of $d(v)$ and linking neighboring vertices by straight-line edges. We will therefore also use v as the center of $d(v)$. We say that a UDR \mathcal{D} preserves the embedding of an embedded graph G with embedding $\mathcal{E}(G)$ if $\mathcal{E}_{\mathcal{D}}(G) = \mathcal{E}(G)$. Let a, b, c be three points in \mathbb{R}^2 . We use $\angle abc$ to denote the clockwise angle defined between the segments ab and bc . We define the angle $\angle d_i d_j d_k$ as the clockwise angle $\angle v_i v_j v_k$ in $\mathcal{E}_{\mathcal{D}}(G)$.

3 NP-Hardness Results

In this section, we prove that recognizing unit disk graphs remains NP-hard for non-embedded outerplanar graphs and for embedded trees. Our proofs apply the

⁴ Note that weak UDRs, in contrast, are not interesting, since a complete graph K_n can easily be represented as a UDR and therefore every graph admits a weak UDR.

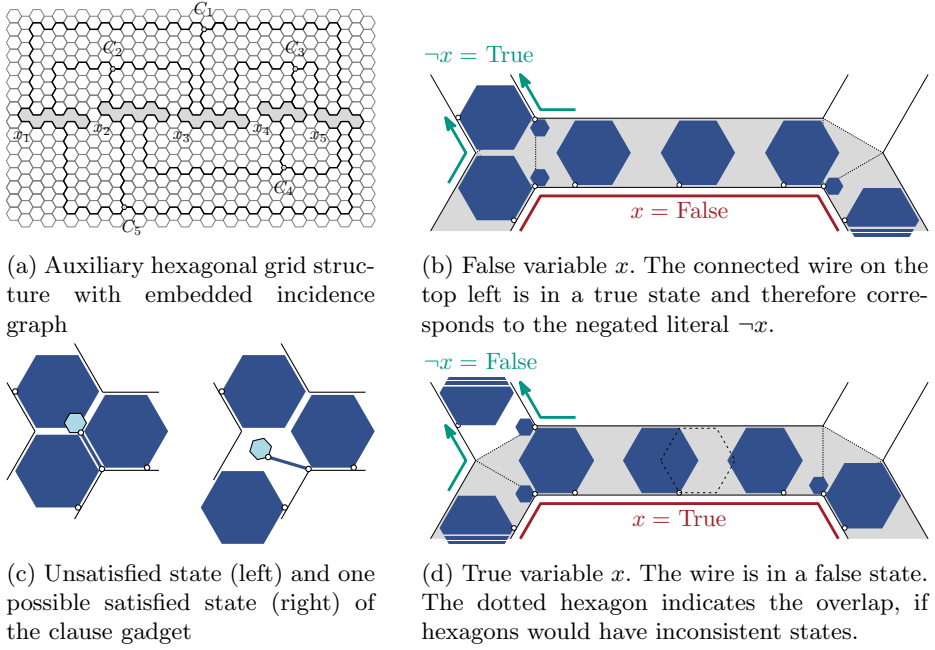


Fig. 2: Auxiliary structure details used by Bowen et al. [1]. All Figures are recreations/adaptions from their paper. The incidence graph is embedded on a hexagonal grid (a). The edges are short corridors in which the blue hexagons are fitted, hinged at white vertices. Hexagons in the variable cycle (red line, grey backdrop) have two states (b) and (d). The clause gadget (c) requires one hexagon, which does not enter the junction.

generic machinery of Bowen et al. [1] to decide realizability of polygonal linkages, which requires to construct gadgets that can model hexagons and rhombi in a stable way. First we sketch the reduction of Bowen et al. (full details in Appendices A.1–A.3), then we describe our constructions of the required stable structures with outerplanar (Section 3.1) and embedded tree gadgets (Section 3.2).

Bowen et al. [1] proved that recognizing unit disk contact graphs is NP-hard for embedded trees, via a reduction from planar 3-SAT, which uses an auxiliary construction formulated as a realization of a polygonal linkage. A polygonal linkage is a set of polygons, which are realizable if they can be placed in the plane, s.t., predefined sets of points on the boundary of these polygons are identified. Bowen et al. define a set of hexagons in a hexagonal tiling (Fig. 2a) with small gaps between them, which form a hexagonal grid, in which a representation of the incidence graph of the planar 3-SAT instance is fitted. Smaller hexagons are fitted into cycles in this grid, s.t., they admit only two different realizations, see Fig. 2b, and determine the state of neighboring small hexagons, see Fig. 2d. The cycles represent variables in a true or false state. The states of the cycles

are transmitted via chains of smaller hexagons into the gaps. The vertex, where three such chains meet, contains a small hexagon on a thin connection, which can only be realized if at least one transmitted state is *true*, see Fig. 2c. The polygonal linkage is realizable if and only if the planar 3-SAT instance is satisfiable. For a detailed description, we refer to Appendix A and Bowen et al. [1]. The building blocks of this reduction are hexagons of variable sizes and short segments. Bowen et al. [1] approximate the hexagons by creating graphs, whose UDCs must be within a constant (asymmetric) Hausdorff distance⁵ of a hexagon and the segments similarly by providing graphs, whose UDCs must be within a constant (asymmetric) Hausdorff distance of long thin rhombi. We extend their notion of λ -stable approximations to UDRs.

Definition 1. *A graph G is a λ -stable approximation of a region P in the plane if, in every UDR of G , there exists a congruence transformation $f : \mathbb{R}^2 \rightarrow \mathbb{R}^2$ such that the union U of all unit disks in the UDR has an asymmetric Hausdorff distance $d_H(f(P), U) \leq \lambda$.*

3.1 Non-embedded Outerplanar Graphs

We prove that recognition of unit disk graphs is hard for non-embedded outerplanar graphs by providing outerplanar graphs G_k^H and G_k^R , which are 7-stable approximations of a hexagon of side length $2k-1$ and a rhombus of width $2k+6$, respectively. Then, the NP-hardness follows immediately from the construction of Bowen et al. [1] sketched above. To obtain the 7-stable approximations we present two graphs, which enforce local bends in one direction of at least π and $\frac{4\pi}{3}$ in any UDR.

A *ladder* L_k (see Figs. 3a and 3c) is a chain of pairwise connected vertices v_i and v'_i , for $i = 1, \dots, k$, also called the *outer* and *inner* vertices of L_k , respectively. Additionally, so-called *extension neighbors*, which are connected to only one outer vertex each, are added on one side of the ladder, s.t., the outer vertices have alternating degrees of four and five. Since the ladder consists of a chain of C_4 's, these neighbors are forced to be placed all on the outside in an outerplanar embedding. The minimal height of such a ladder is $2\sqrt{3} + 2 - \varepsilon$, which is the height of the smallest bounding box of a tight packing of three rows of unit disks minus an (arbitrarily) small constant $\varepsilon > 0$.

The permission of overlap between adjacent disks allows for a placement of one extension neighbor almost on top of its adjacent outer vertex, which leads to an ever so slight inwards bend and, more importantly, any outwards bend is impossible. In order to enforce an inward bend of at least $\frac{4\pi}{3}$, we connect the last inner vertex u_j^1 of one ladder with the first inner vertex u_1^2 of a second ladder and the last and first outer vertex v_j^1/v_1^2 of the first and second ladder, respectively, both with a vertex v_c , which has three attached extension neighbors, see Fig. 3b. This construction is called a *corner connector*. Since it

⁵ Recall that the asymmetric Hausdorff distance from a set A to a set B in a metric space with metric d is defined as $d_H(A, B) = \sup_{a \in A} \inf_{b \in B} d(a, b)$.

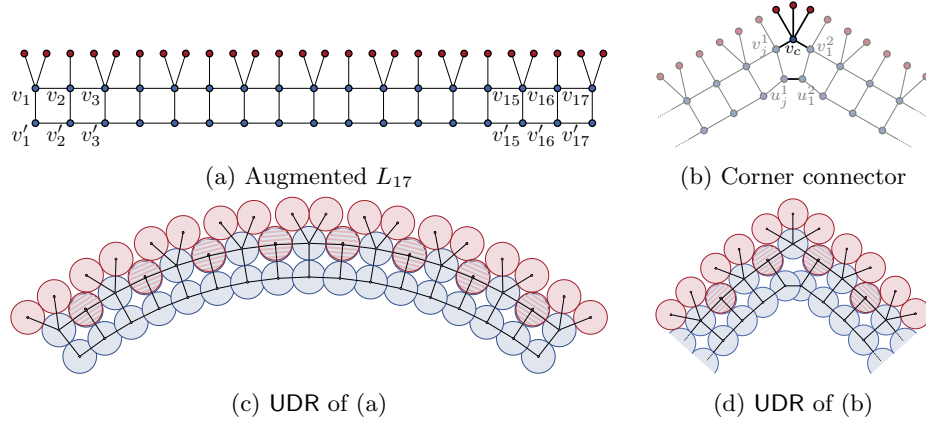


Fig. 3: Components for creating λ -stable approximations G_k^H and G_k^R . Ladder L_{17} (a) and its UDR (c), as well as a corner connector (b) and its UDR (d). The corner connector connects two ladders (lighter colored parts) and its actual parts have a darker color in (b). The bends in the UDRs are required but exaggerated.

is impossible to place the disk of any extension neighbor of v_c inside the 5-cycle $d(v_j^1), d(u_j^1), d(u_1^2), d(v_1^2), d(v_c)$, without overlapping at least two disks in the UDR, all extension neighbors are still forced to the outside and therefore $\angle v_j^1 v_c v_1^2 > \frac{4\pi}{3}$, see Fig. 3d.

Placing two ladders opposite each other and connecting them on one end with three corner connectors as shown in Fig. 4, yields a 7-stable approximation G_k^R of a thin rhombus. The following lemma is analogue to Lemma 10 in [1].

Lemma 1 (\star). *For every positive integer k the outerplanar graph G_k^R in Fig. 4 is a 7-stable approximation of a rhombus of width $2k + 6$ and height $6\sqrt{3} + 2$.*

Proof (Sketch). The graph G_k^R is made up of components, which make any bend to the outside impossible, see Fig. 4a. Since two ladders need to be overlap free, the minimum height of the ladders guarantees that part of the boundary of the union over all disks in the UDR of G_k^R lies above and below the line $\overline{c_0 l_0}$, see Fig. 4b. The largest vertical distance of the rhombus to this line is $3\sqrt{3} + 1 \approx 6.196 < 7$.

Lemma 2 (\star). *For every integer $k = 6n + 4, n \in \mathbb{N}$, the outerplanar graph G_k^H in Fig. 5a is a 7-stable approximation of a regular hexagon of side length $2k - 1$.*

Proof (Sketch). The 7-stable approximation G_k^H of a hexagon of side length $2k - 1$ uses again ladders and corner connectors to trace the outline of the hexagon. Then the inside of this construction is filled with a set of ladders until no additional ladders can be added, see Fig. 5a. Outwards bends are impossible by construction of the ladders and corner connectors and inwards bends are

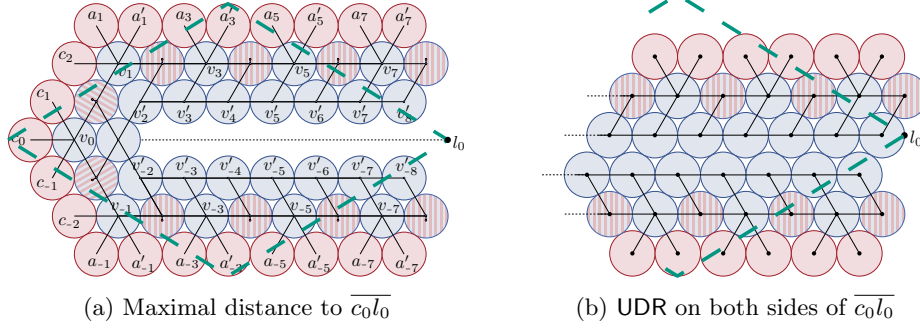


Fig. 4: A 7-stable approximation G_7^R of a rhombus superimposed on its UDR. The maximal distance of any point of the UDR to $\overline{c_0 l_0}$ is smaller or equal 7 (a) and at all points of $\overline{c_0 l_0}$ a part of the UDR lies above and below $\overline{c_0 l_0}$ (b). Both UDRs require a small inward bend to be valid and hatched disks indicate almost overlapping placement of a red disk on a blue disk, with a small shift to the outer side. Both inward bends and outward shifts are omitted.

strongly limited since the interior of the hexagon is almost completely filled with ladders. Since the amount of compression in a ladder is very limited, this leaves only a constant amount of space on the inside of a UDR of G_k^H .

Theorem 1. *Recognizing unit disk graphs is NP-hard for outerplanar graphs.*

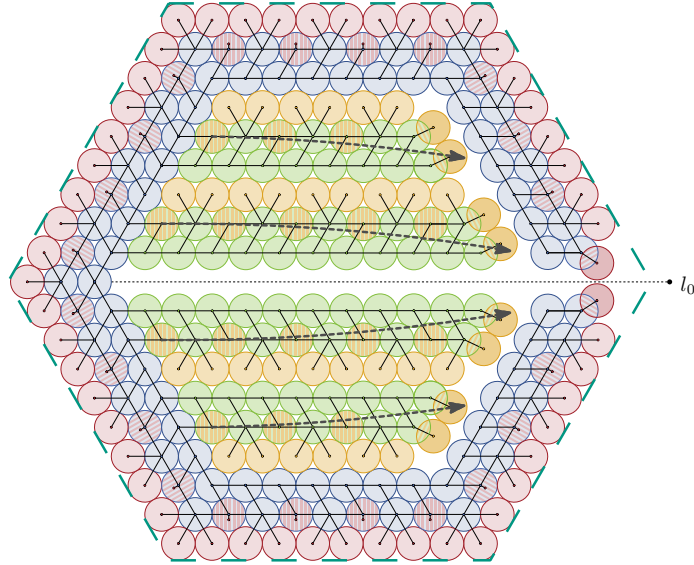
Proof. This result follows from Lemmas 1 and 2 by using the polygonal linkage reduction of Bowen et al. [1] (see also Appendix A). Note that we can emulate hinges exactly as in the original reduction.

3.2 Embedded Trees

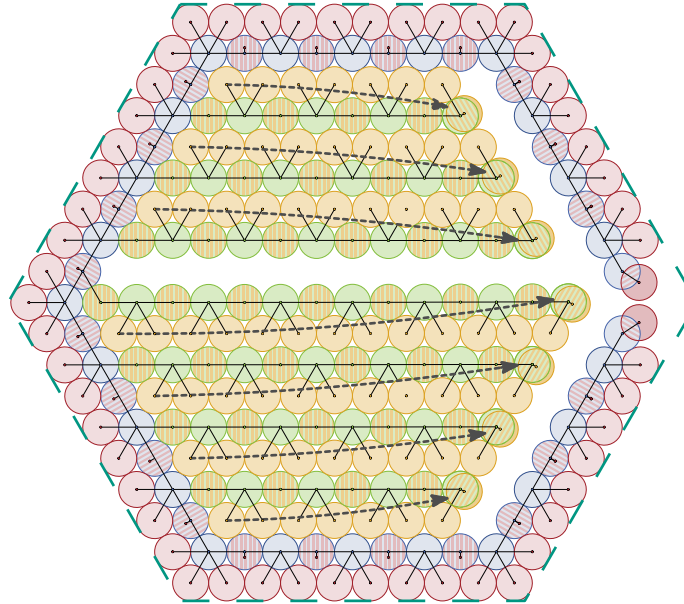
By slightly adapting the construction of the outerplanar graphs of Section 3.1, we can prove that recognizing unit disk graphs is NP-hard for embedded trees. The crucial observation is that we used the outerplanarity of G_k^R and G_k^H exclusively to be able to build a tree-like structure out of chains of 4- and 5-cycles. We used this to force the placement of leaf disks to a specific side of these chains in any UDR of G_k^R and G_k^H . As we are concerned with embedded trees in this section, we can omit the inner vertices of the ladder, as the given embedding puts the leaves on the desired side of the chains. This results in a tree. We call a ladder without the inner vertices a *chain*.

We can now use a very similar construction idea as for G_k^R and G_k^H above. We need to augment both gadgets with an additional chain in order to retain the property, that no parts of these gadgets can be folded onto themselves. The resulting trees T_k^R and T_k^H are shown in Figs. 5b and 6. A more detailed description can be found in the proof of Theorem 2 in Appendix A.5.

Theorem 2 (*). *Recognizing unit disk graphs is NP-hard for embedded trees.*



(a) Combination of the ladder and corner connectors into 7-stable approximation G_k^H of a hexagon superimposed on its UDR.



(b) A 7-stable approximation tree T_k^H of a hexagon superimposed on its UDR.

Fig. 5: 7-stable hexagon approximations. Hatched disks indicate almost overlapping placement of disks. Necessary infinitesimal bends are omitted. The bend directions of the inner components are indicated with gray arrows. The approximated regular hexagon is indicated by the dashed green outlines.

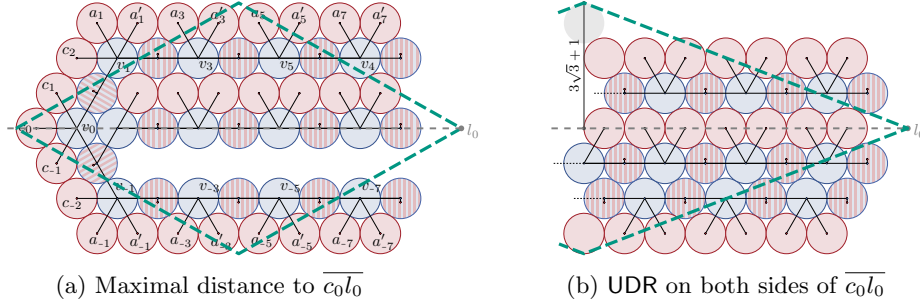


Fig. 6: A 7-stable approximation T_k^R of a long thin rhombus superimposed on its UDR. The maximal distance of any point of the UDR to $\overline{c_0 l_0}$ is smaller or equal 7 (a) and at all points of $\overline{c_0 l_0}$ a part of the UDR lies above and below $\overline{c_0 l_0}$ (b). In both cases at any point along $\overline{c_0 l_0}$ at least one point on the boundary of the union of all disks in a UDR of T_k^R lies on or above $\overline{c_0 l_0}$ and on or below $\overline{c_0 l_0}$.

4 Recognition Algorithm for Caterpillars

We propose a linear-time algorithm using similar ideas to Klemz et al. [12], that recognizes if an input caterpillar graph $G = (V, E)$ admits a UDR or not; it is constructive and provides a representation if one exists. However, we need to address several new issues as we show that a larger class of graphs admits a UDR compared to a UDC. Clearly, if G contains a vertex of degree at least 6, then due to the unit disk packing property, it does not admit a UDR. Hence, every realizable caterpillar must have maximum degree $\Delta \leq 5$. Moreover, it is easy to observe that all caterpillars with $\Delta \leq 4$ admit a UDC (and thus a UDR), as also noted by Klemz et al. [12]. Not every caterpillar with $\Delta = 5$, however, is realizable as UDR. We show that two consecutive degree-5 vertices on B_G cannot be realized. The following lemma gives a sufficient condition for a “No” instance to be used in the recognition algorithm. The proof of Lemma 3 is stated in Appendix B.1.

Lemma 3 (*). *If B_G contains two adjacent degree 5 vertices u, v , then it does not admit a unit disk intersection representation.*

4.1 The Algorithm

As a preprocessing step we augment all backbone vertices of degree 3 or lower with additional degree-1 neighbors, s.t., they have degree 4. Consider a chain v_1, \dots, v_n of backbone vertices. Now assume all vertices are of degree 4 or lower. We place them on a horizontal line. For each $1 \leq i \leq n$ at disk $d(v_i)$, we place its leaf neighbor disks $d(v_i^t), d(v_i^b)$ first at the top and then at the bottom of $d(v_i)$, see Fig. 7a, s.t., the clockwise angle $\angle v_i^t v_i v_i^b = \frac{4\pi}{3} - 2i\varepsilon$. The rotational ε offset avoids adjacencies between the leaf disks. While these offsets can add up, we can choose ε small enough for every finite caterpillar, s.t., this is negligible.

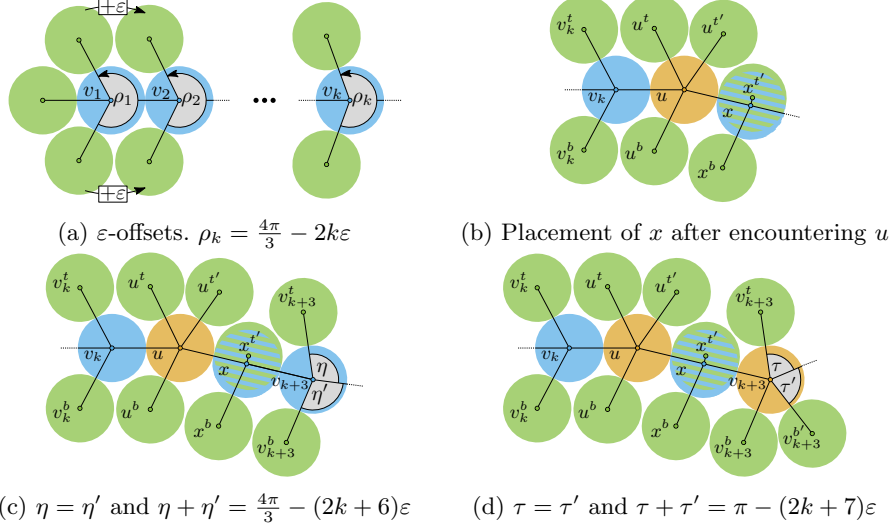


Fig. 7: Chains of degree-4 vertices are placed in a dense packing formation with small offsets (a). A degree-5 vertex places an additional leaf on one side (b). The next vertex v_{k+3} can again be placed with the desired angle of just over $\frac{2\pi}{3}$ between two neighbors (c). Placement of v_{k+3} is possible if its degree is 5 (d). Note that, the rotational offset angles are exaggerated, for better readability.

Now we assume that not all vertices are of degree 4 or lower. To keep the entire construction of the backbone x -monotone, whenever we encounter a degree 5 vertex u after a degree four vertex v_k , we place $d(u^{t'})$ of its additional leaf $u^{t'}$ alternately on the top or the bottom side with a $\frac{\pi}{3} + \varepsilon$ rotational offset to $d(u^t)$ (or $d(u^b)$). We will assume that we placed the disk at the top. Therefore $\angle u^{t'}uu^b \leq \pi - (2k+1)\varepsilon$, i.e., an almost horizontal connection, see Fig. 7b.

If the next vertex x has also degree five, then due to Lemma 3 we know that the sequence is not realizable. Otherwise, we place $d(x)$, s.t., it is touching $d(u)$ with a $\frac{\pi}{3} + \varepsilon$ rotational offset to $d(x)$, see Fig. 7b. We place $d(x^b)$ at the planned position relative to $d(x)$ at the bottom, i.e., with a $\frac{\pi}{3} + (k+2)\varepsilon$ counterclockwise offset relative to the x -axis, however, we place $d(x^t)$ almost exactly on top of $d(x)$ with a very small shift of $\frac{\varepsilon}{C_n}$ orthogonal to \overline{ux} , for some large constant C . This prevents touching of $d(u)$ and $d(x^t)$, without creating an adjacency between $d(u^{t'})$ and $d(x^t)$.

From this point onwards, we consider the direction of \overline{ux} to be the direction in which we extend the backbone of the caterpillar. Any following disk $d(v_{k+3})$ can be placed again in the new extension direction touching $d(x)$. Its leaf disks $d(v_{k+3}^t)$ and $d(v_{k+3}^b)$ can be placed in their planned positions, i.e. with a clockwise or counterclockwise offset of $\frac{\pi}{3} + (k+3)\varepsilon$ relative to the new extension direction, respectively, which results in a clockwise angle $\angle u_tuu_b \leq \frac{4\pi}{3} - (2k+6)\varepsilon$. Note

that v_{k+3} can have a degree of four (Fig. 7c) or five (Fig. 7d) and that at this point, if v_{k+3} has degree five, we can immediately repeat this procedure.

As a postprocessing step, we remove all degree-1 vertices that were added in the preprocessing step. Then from the above description of the algorithm and the correctness analysis in Appendix B.2 we obtain the following theorem.

Theorem 3. *Let $G = (V, E)$ be a caterpillar graph. G admits a UDR if and only if G does not contain any two adjacent degree-5 vertices in the backbone path B_G of G . This property can be tested in linear time and if a UDR exists then it can be constructed in linear time.*

5 Weak UDCs of Lobsters on the Triangular Grid

We have shown that recognition of UDRs is NP-hard for outerplanar graphs and linear-time solvable for caterpillars, which mirrors the results for UDCs and weak UDCs; it leaves the recognition complexity for (non-embedded) trees as an open question for both UDRs and UDCs. For weak UDCs, however, recognition has been proven NP-hard for trees [7]. In order to investigate the complexity of weak UDCs further, we zoom in on the gap between trees and caterpillars and investigate the graph class of lobsters.

The *spine* of a weak UDC of a lobster G is the polyline defined by connecting the centers of all disks belonging to the vertices of B_G in order. A weak UDC is *straight*, if its spine is a straight line segment. Similarly, a weak UDC is *x-* or *y-monotone*, if its spine is *x-* or *y-monotone*. Since we consider weak UDCs with contacts between non-adjacent disks permitted, we focus our attention on weak UDCs placed on a triangular grid (similarly to previous work on weak UDCs [7]).

5.1 Straight Backbone Lobsters

Since any caterpillar G , admits a weak UDC if and only if it admits a straight weak UDC [7] we investigate lobster graphs, which admit a straight weak UDC. These are not all lobsters, since any simple lobster graph containing a non-backbone vertex of degree 6 only admits a non-straight weak UDC. We observe that already for this restricted subclass, a greedy placement scheme similar to Cleve's approach [7] for caterpillars is not possible; again shown by an example.

We specify two lobster graphs G and G' , see Fig. 8. It can be checked via exhaustive enumeration that G admits 18 different weak UDCs, while G' admits only 12. The subgraphs induced by their first three backbone vertices are identical, however the realization of the descendants of v_3 (highlighted in red) is unique for both graphs (up to symmetry) and dependent on the structure of the graphs beyond this point. We can therefore not simply scan over the backbone in a greedy manner and fix all positions for the disks of descendants of a backbone vertex and then continue on to the next. It is, however, still possible to do this in linear time with dynamic programming. The requirements for this are actually less strict, as it is already sufficient to have a strictly *x-monotone* rather than a straight backbone, which we show in the next section.

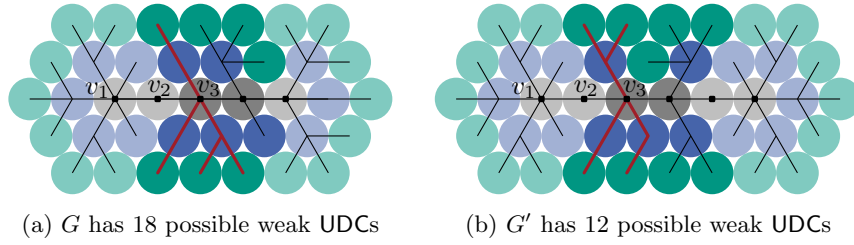


Fig. 8: The subgraphs of G and G' induced by their first three backbone vertices are equal, however, depending on the following vertices a different realization of the neighbors of v_3 is necessary.

5.2 Monotone Weak UDCs

If we can guarantee that a lobster can be realized as a strictly x -monotone weak UDC, we can compute such a weak UDC with a linear-time dynamic programming algorithm. The dynamic program uses the following three observations.

Observation 1 (\star). *The number of possible placements of a backbone vertex v_i and its descendants is constant for a fixed position of v_i .*

Observation 2 (\star). *For a fixed grid position, the number of backbone vertices of a strictly x -monotone weak UDC, who can occupy this position by themselves or with a descendant is constant. Moreover, the distance in graph between the first and the last such vertex is constant.*

Observation 3 (\star). *Let C be a sufficiently large constant, and let A, B be two weak UDC, whose last C backbone vertices have placed themselves and their descendants in such a manner, that the pattern of occupied grid positions and the placement of the last backbone vertex is equivalent up to translation and rotation. Then any extension graph C , which can be appended to A , s.t., the combined graph admits a weak UDC can also be appended to B , s.t., their combined graph admits a weak UDC and vice versa.*

With these three claims we obtain the following Lemma.

Lemma 4 (\star). *Using dynamic programming it can be checked in linear time if a lobster graph admits an x -monotone weak UDC on the triangular grid.*

5.3 General Lobsters

The algorithm sketched in the previous section recognizes lobster graphs, which admit a strictly x -monotone weak UDC in linear time. Now we set out to prove that every lobster which admits a weak UDC also admits a strictly x -monotone weak UDC. We prove this by induction. The induction step is done as a computer-assisted proof. See Appendix D for details.

Lemma 5. *Every lobster graph, which admits a weak UDC on the triangular grid, also admits an x -monotone weak UDC on the triangular grid.*

Proof. We use induction on the length of the backbone. The base cases are backbones of length one, two or three. The spine of any realization is at most a polyline consisting of two segments and can therefore always be rotated to be x -monotone. The induction hypothesis is, that any lobster graph, with a backbone of length k admits an x -monotone weak UDC. In the induction step we need to show that any extension to a graph G' with a backbone of length $k + 1$, can be realized as a weak UDC if and only if it can be realized in an x -monotone way. The extensions are done by appending a single new backbone vertex v_{k+1} , whose descendants are specified as a sorted list of the degrees of its direct neighbors. Since the total degree of every vertex is at most 6, the set Γ of options for v_{k+1} is constant (Observation 1). Let Θ be the set of possible combinations of already occupied grid positions where v_{k+1} is placed such that the spine remains x -monotone. Let Δ_6 and Δ_3 be the sets of possible placements of disks of descendants of v_{k+1} , when v_{k+1} is placed at one of six (in the unrestricted case) or one of three (in the strictly x -monotone case) positions. Therefore we can enumerate all triples $(\gamma \in \Gamma, \delta_3 \in \Delta_3, \theta \in \Theta)$ and $(\gamma \in \Gamma, \delta_6 \in \Delta_6, \theta \in \Theta)$ and check if they are realizable. By exhaustive enumeration,⁶ we have found that for every possible $(\gamma, \delta_6, \theta)$, which is realizable, we can find a suitable $(\gamma, \delta_3, \theta)$, which is realizable, too. This concludes the induction step.

From Lemmas 4 and 5, we conclude the following theorem.

Theorem 4. *It can be decided linear time if a lobster graph admits a weak UDC on the triangular grid.*

6 Conclusions

We have investigated the existing complexity gap for the recognition problem of UDRs and weak UDCs. In addition to the open problems for various graph classes in different settings (recall Table 1 in Section 1) there are two main open questions. First, we have investigated weak UDCs of lobsters on the triangular grid, however, it is not entirely clear if every lobster, which admits a weak UDC, also does so on the grid. Second, it seems reasonable to assume that our enumeration approach can be extended to graph classes beyond lobsters, which admit a weak UDC at least on the triangular grid. In fact, we conjecture that every class of trees, in which each vertex has bounded distance to a central backbone in extension of caterpillars and lobsters, can be recognized in polynomial time by such an approach.

⁶ The cases were reduced, by considering symmetry and infeasibility beforehand. Enumeration was done in the form of a computer-assisted proof. Details are explained in Appendix D

Acknowledgements. We thank Jonas Cleve and Man-Kwun Chiu for fruitful discussions about the project during their research visits in Vienna.

References

1. Bowen, C., Durocher, S., Löffler, M., Rounds, A., Schulz, A., Tóth, C.D.: Realization of simply connected polygonal linkages and recognition of unit disk contact trees. In: Graph Drawing and Network Visualization (GD’15). LNCS, vol. 9411, pp. 447–459. Springer International Publishing (2015). https://doi.org/10.1007/978-3-319-27261-0_37
2. Breu, H., Kirkpatrick, D.G.: On the complexity of recognizing intersection and touching graphs of disks. In: Brandenburg, F.J. (ed.) Graph Drawing (GD’95). LNCS, vol. 1027, pp. 88–98. Springer (1996). <https://doi.org/10.1007/BFb0021793>
3. Breu, H., Kirkpatrick, D.G.: Unit disk graph recognition is NP-hard. *Comput. Geom. Theory Appl.* **9**(1–2), 3–24 (1998). [https://doi.org/10.1016/S0925-7721\(97\)00014-X](https://doi.org/10.1016/S0925-7721(97)00014-X)
4. Chalopin, J., Gonçalves, D., Ochem, P.: Planar graphs have 1-string representations. *Discrete & Computational Geometry* **43**(3), 626–647 (2010). <https://doi.org/10.1007/s00454-009-9196-9>
5. Chaplick, S., Ueckerdt, T.: Planar graphs as VPG-graphs. In: Didimo, W., Patrignani, M. (eds.) Graph Drawing (GD’12). LNCS, vol. 7704, pp. 174–186. Springer (2013). https://doi.org/10.1007/978-3-642-36763-2_16
6. Chiu, M., Cleve, J., Nöllenburg, M.: Recognizing embedded caterpillars with weak unit disk contact representations is NP-hard. *CoRR* **abs/2010.01881** (2020)
7. Cleve, J.: Weak unit disk contact representations for graphs without embedding. *CoRR* **abs/2010.01886** (2020)
8. Felsner, S.: Rectangle and square representations of planar graphs. In: Pach, J. (ed.) *Thirty Essays on Geometric Graph Theory*, pp. 213–248. Springer (2013). https://doi.org/10.1007/978-1-4614-0110-0_12
9. Gonçalves, D., Isenmann, L., Pennarun, C.: Planar graphs as L-intersection or L-contact graphs. In: *Discrete Algorithms (SODA’18)*. pp. 172–184. SIAM (2018). <https://doi.org/10.1137/1.9781611975031.12>
10. Hliněný, P.: Classes and recognition of curve contact graphs. *Journal of Combinatorial Theory, Series B* **74**(1), 87–103 (1998). <https://doi.org/10.1006/jctb.1998.1846>
11. Hliněný, P., Kratochvíl, J.: Representing graphs by disks and balls (a survey of recognition-complexity results). *Discrete Mathematics* **229**(1), 101–124 (2001). [https://doi.org/10.1016/S0012-365X\(00\)00204-1](https://doi.org/10.1016/S0012-365X(00)00204-1)
12. Klemz, B., Nöllenburg, M., Prutkin, R.: Recognizing weighted disk contact graphs. In: Graph Drawing and Network Visualization (GD’15). LNCS, vol. 9411, pp. 433–446. Springer International Publishing (2015). https://doi.org/10.1007/978-3-319-27261-0_36
13. Koebe, P.: Kontaktprobleme der konformen Abbildung. *Ber. Sächs. Akad. Wiss. Leipzig, Math.-Phys. Klasse* **88**, 141–164 (1936)

A Omitted Details of Section 3

Bowen et al. [1] proved that recognizing unit disk contact graphs is NP-hard for embedded trees, via a reduction from planar 3-SAT, which uses an auxiliary construction formulated as a realization of a polygonal linkage. Polygonal linkages are explained in Appendix A.1. The details of this auxiliary structure are explained in Appendix A.2. Then a tree, whose UDC is an approximation of the auxiliary structure and which mimics the shape and behaviour of it, is constructed. This construction is summarized in Appendix A.3.

A.1 Polygonal Linkages

Bowen et al. [1] considered multiple problems in their work, one of which is the *polygonal linkage realizability* (PLR) problem. A polygonal linkage is a set \mathcal{P} of convex polygons and a set H of hinges. One hinge is a set of two or more points on the boundaries of distinct polygons. A polygonal linkage is realizable, if every $p \in \mathcal{P}$ can be placed in the plane, s.t.

- all polygons are interior disjoint
- for every hinge $h \in H$, all points of the hinge coincide and
- a predefined cyclic order of adjacent polygons around every hinge is kept.

In our case and in the case of this reduction, hinges are only of size two, i.e., a realization will identify exactly two points on distinct polygons per hinge. This means that cyclic order around hinges is always kept by default. A polygonal linkage and its realization are shown in Fig. 9.

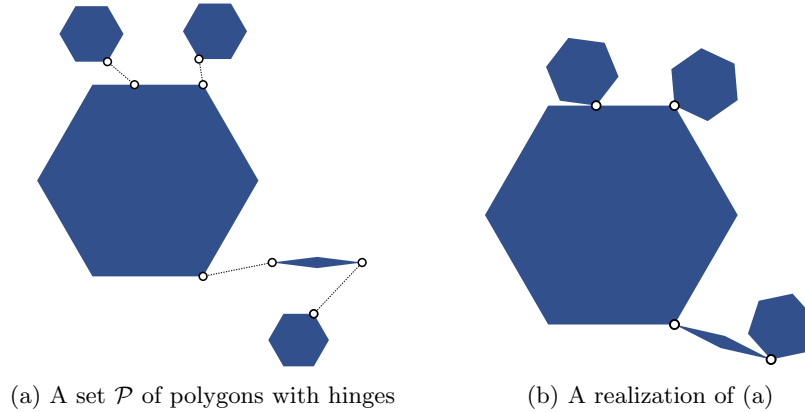


Fig. 9: An instance of PLR (a), where points belonging to the same hinge are indicated with a dotted line connection. A placement of (rotated and/or translated) copies of the polygons in \mathcal{P} in the plane is a realization (b) if the points of the same hinge are identified.

A.2 Auxiliary Structure

The auxiliary structure mimics a hexagonal grid. This grid-like structure is obtained by using a hexagonal tiling of the plane and then shrinking every hexagon by a small amount to obtain narrow channels of a fixed height between two hexagons, where ε is a sufficiently small constant. At the corners of the hexagons, three such channels meet to form a junction. The union of all channels and junctions forms the grid-like structure. In this grid, a representation of the incidence graph G_ϕ of the planar 3-SAT instance ϕ is fitted, see Fig. 2a.

A variable v of ϕ is represented in this grid as an alternating cycle of channels and junctions, indicated with a grey fill in Fig. 2a. In such a cycle the channels can be filled with smaller hexagons of height h , which are connected to the large hexagon on the side of the channel – which is on the “inside” of the variable cycle – via a junction. In a channel, one corner of each of the small hexagons is connected to the large hexagon via a hinge, s.t., the small hexagon can be “flipped” around this junction. Due to the chosen size, the hexagon can be realized in one of two states, see Figs. 2b and 2d. The distance of the hinges of neighboring small hexagons is chosen in such a way that the state of one hexagon determines the state of all hexagons in the channel, see Fig. 2d. At each junction, we add an even smaller hexagon with a hinge to the corner of that large hexagon, which is adjacent to the channels on either side of the junction in the variable cycle. This propagates the state of the hexagons in one channel through the junction into the other channel and so throughout the entire cycle. See Figs. 2b and 2d for a detailed explanation.

Wire gadgets are alternating paths of channels and junctions, which use the same mechanism to propagate the state of the hexagons in the channels and therefore admit two states overall.

Wire gadgets can be connected to a variable cycle at every junction using the third unoccupied channel and adding a second very small hexagon in the junction. A wire gadget is considered to transmit the value *true*, if and only if, part of the first small hexagon of the first channel of the wire gadget enters into the junction. By placing the small hexagon on one or the other corner (cf. Figs. 2b and 2d) the truth value which is transmitted can be “inverted” if necessary.

For every clause in ϕ , three such wire gadgets are connected to the variable cycles of the occurring variables and the wires are routed to meet in a junction. This junction contains a small hexagon connected to the corner of a large hexagon via a long and very thin rhombus (in place of a line segment), s.t., an overlap-free realization is only possible, if at least one connected wire gadget has no hexagon entering the junction and is therefore in a true state, see Fig. 2c.

In order to guarantee a somewhat rigid placement of these hexagons, the entire construction is surrounded by a set of six huge hexagons, and the hexagons acting as the faces of the hexagonal grid are column-wise connected (cf. Fig. 10). This restricts the position of the large hexagons to an N -neighborhood, where N is a polynomial of the number of variables and clauses in ϕ [1].

Note that the connections between the polygons in the polygonal linkage induce a tree. In particular note that we can replace the hexagons with outer-

planar graphs and replace the hinges between them with paths of length one to three and the entire construction remains an outerplanar graph. The same way we can replace all hexagons with trees and replace the hinges with vertex paths of length one to three and the entire construction remains a tree.

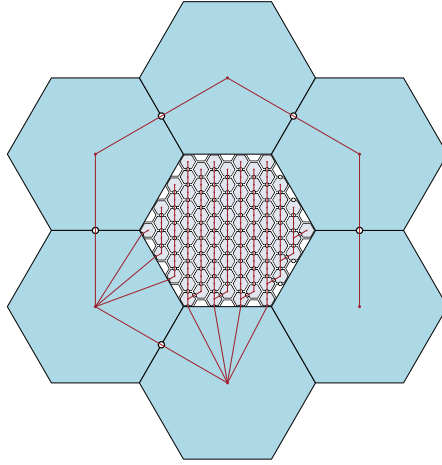


Fig. 10: The composition of the rigid structure as a realization of a polygonal linkage. Hinges are indicated by points. The figure is a recreation of a similar figure in [1], augmented with lines, which emphasize the tree-like structure of connections in the polygonal linkage.

For a more detailed description, a full construction and the proof of the semi-rigid placement we refer to the original paper of Bowen et al. [1].

A.3 Approximating the Auxilliary Structure

In order to prove the NP-hardness for recognition of unit disk contact graphs, Bowen et al. [1] created λ -stable approximations of the basic building blocks of the auxiliary structure (hexagons of varying sizes and long thin rhombi). A graph is a λ -stable approximation of a polygon P , if the boundary union of all disks in its UDC is necessarily within a constant asymmetric Hausdorff distance λ of a congruent copy of P .

Bowen et al. described the construction procedures for two graphs T_k, T'_k , which are 2-stable approximations of a long thin rhombus and a regular hexagon. These two graphs are shown in Fig. 11. For the details of these constructions, we again refer to Bowen et al. [1]. The construction of our building blocks using

outerplanar graphs in Section 3.1 and embedded trees Section 3.2 is based on these graphs.

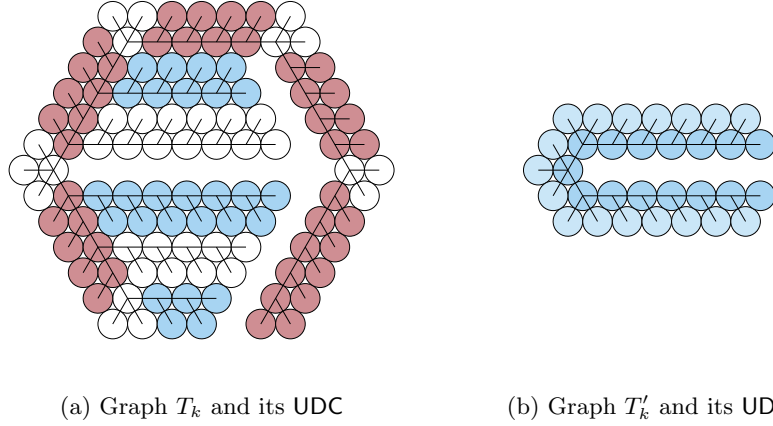


Fig. 11: The 2-stable approximations of a long thin rhombus (a) and a regular hexagon (b). All Figures are recreations from Bowen et al. [1].

It remains to discuss how the hinges are modeled. Two λ -stable approximations G, G' of two polygons P, P' are connected with a path of vertices of constant length, if there exists a hinge $h \in H$, with one point on the boundary of P and the other on the boundary of P' . The exact length of the path is dependent on the location of the hinge. If the hinge is not placed on a corner of either polygon, they are simply connected via a single cut vertex, and with a path of length three otherwise, in order to facilitate more movement, which mimics the possibility of polygons to rotate around hinges. The union of the UDC of two thus connected graphs G, G' , remains a constant factor approximation of a congruent copy of the realization of $P \cup P'$.

A.4 Proofs of Lemmas 1 and 2

To prove Lemmas 1 and 2 we need to establish some initial Lemmas. First a ladder L_k consists of two paths v_1, v_2, \dots, v_k and v'_1, v'_2, \dots, v'_k of vertices – also called the *outer* and *inner* vertices respectively – s.t., each pair (v_i, v'_i) is connected with an edge. The blue vertices in Fig. 3a form a ladder, specifically L_{17} . A UDR of L_{17} is shown in the blue disks of Fig. 3c.

Lemma 6. *Let $k \in \mathbb{N}$ and let \mathcal{D} be a UDR of L_k . Then $\mathcal{E}_{\mathcal{D}}(L_k)$ induces the same embedding as shown in Fig. 3a, which is outerplanar.*

Proof. Clearly no disk can be placed inside a UDR of a C_4 , without intersecting at least two disks of the C_4 . Since every disk $d(v_i)$ of a vertex v_i , which is not

part of the C_4 intersects at most one disk of the C_4 , this is impossible and the outer face is fixed. Therefore the induced embedding is unique.

Lemma 6 implies that we can assign a clear “outer side”, i.e., $d(v_1), \dots, d(v_k)$ and “inner side”, i.e., $d(v'_1), \dots, d(v'_k)$ to a UDR of L_k .

Next we want to ensure that any overall bend towards the outer side is impossible. For this we will augment L_k with additional neighbors. We restrict the ladders to an odd length and alternatingly add one and two leaf neighbors, which we will call extension neighbors. The resulting graph can be seen in Fig. 3a.

Lemma 7. *Let $(v_1, v_2, v_3, v_4, v_5)$ be a chain of vertices on the outer side of a ladder L_k with one, two, one, two and one extension neighbor respectively. Then the sum of angles $\gamma = \angle v_3 v_2 v_1 + \angle v_4 v_3 v_2 + \angle v_5 v_4 v_3$ in a UDR of L_k is smaller than 3π , i.e., overall we bend more towards the inner side than towards the outer side.*

Proof. We will refer to the two extension neighbors of v_2 as a and a' , both of which are placed on the outer side of the ladder. Similar we will call the extension neighbors of v_4 , b and b' . The singular extension neighbor of v_3 , will be referred to as c . The naming is also shown in Fig. 12a. Without loss of generality, we assume that the clockwise order on v_2 is (v_1, a, a', v_3, v'_2) and analogue the clockwise order on v_4 is (v_3, b, b', v_5, v'_4) . Figs. 12a and 12c depict this placement and its UDR.

First observe that $\angle v_1 v_2 a > \frac{\pi}{3}$, since $|v_1 v_2| \leq 2$, $|v_2 a| \leq 2$ and $|v_1 a| > 2$. For the same reason we have $\angle a v_2 a' > \frac{\pi}{3}$ and $\angle a' v_2 v_3 > \frac{\pi}{3}$. This means that

$$\angle v_1 v_2 v_3 = \angle v_1 v_2 a + \angle a v_2 a' + \angle a' v_2 v_3 > \pi$$

and similarly $\angle v_3 v_4 v_5 > \pi$.

Now we will distinguish two extremes at v_3 . In the first extreme position $d(c)$ is placed almost on top of $d(v_3)$, s.t., $\angle v_2 v_3 c = \angle c v_3 v_4 = \alpha$ and α tends toward $\frac{\pi}{2}$ as $|v_3 c|$ approaches 0. The extreme placement with $|v_3 c|$ equal to 0 is shown in Fig. 12d. This results in $\angle v_2 v_3 v_4 > \pi$. To reach the second extreme (cf. Fig. 12e) $d(c)$ is moved outwards. As $|v_3 c|$ increases, it facilitates a local outward bend and an angle $\angle v_2 v_3 v_4 > \pi - \varphi$, where $\varphi = \cos^{-1} \left(\frac{|v_2 c|^2 + |v_2 v_3|^2 - |v_3 c|^2}{2|v_2 c||v_2 v_3|} \right)$, see Fig. 12b. However, in order to maximize this bend, v_2 and v_4 are moved into the resulting gap between v_3 and c , s.t., the distances $|v_2 c|$ and $|v_4 c|$ are equal to $2 + \varepsilon'$, where ε' is a very small constant. In particular we have $\angle a' v_2 c > \frac{\pi}{3}$, and similarly $\angle c v_4 b > \frac{\pi}{3}$. Finally this leads to the following values:

$$\angle v_1 v_2 v_3 = \angle v_1 v_2 a + \angle a v_2 a' + \angle a' v_2 c + \angle c v_2 v_3 \geq \frac{\pi}{3} + \frac{\pi}{3} + \frac{\pi}{3} + \varphi = \pi + \varphi$$

$$\angle v_3 v_4 v_5 = \angle v_3 v_4 c + \angle c v_4 b + \angle b v_4 b' + \angle b' v_4 v_5 \geq \varphi + \frac{\pi}{3} + \frac{\pi}{3} + \frac{\pi}{3} = \pi + \varphi$$

Clearly the overall bend towards the inside is minimized, if φ and therefore $|v_3 c|$ is minimal, i.e., we are as close as possible to the first extreme state. Since $|v_3 c| > 0$, we have $\angle v_2 v_3 v_4 > \pi$ and finally

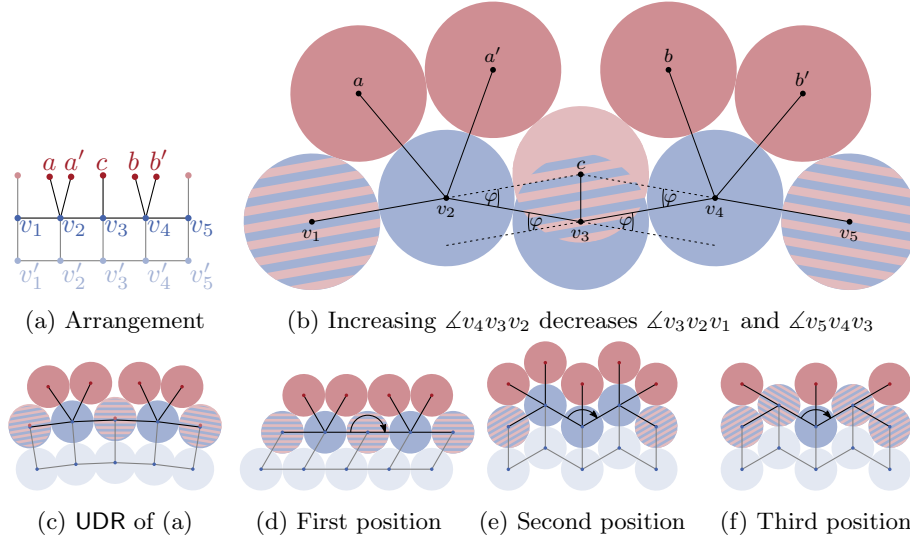


Fig. 12: Figures for Lemma 7. (a) Is the graph as stated in Lemma 7. (b) If $d(c)$ is moved outwards to facilitate an angle $\angle v_4 v_3 v_2 = \pi + \varphi$, i.e., a local outwards bend, it enforces at the same time an inwards bend of φ at $\angle v_3 v_2 v_1$ and $\angle v_5 v_4 v_3$. (c) A valid UDR of (a) including the ε gaps between disks, when necessary. (d-f) Extreme positions of (c), s.t., $\angle v_2 v_3 v_4 = \pi$ (d) or $\angle v_2 v_3 v_4 = \frac{2\pi}{3}$ (e-f).

$$\gamma = \angle v_1 v_2 v_3 + \angle v_2 v_3 v_4 + \angle v_3 v_4 v_5 > 3\pi$$

Note that the second extreme position can also be achieved by using more overlap between $d(v_2)$ or $d(v_4)$ and one of their extension neighbors, however, this configuration forces $\angle a v_2 v_3$ and $\angle v_3 v_4 b'$ to approach π and therefore results in a similar overall inwards bend by φ , as shown in Fig. 12f.

We can also add a third extension neighbor to an outer vertex of a ladder to force an even more pronounced bend towards the inside. The corresponding graph construction is shown in Fig. 3b and a valid UDR in Fig. 3d.

Lemma 8. *Let (v_1, v_2, v_3) be a chain of outside vertices of a ladder, s.t., v_2 has degree 5, i.e., 3 extension neighbors. Then the angle $\angle v_3 v_2 v_1$ is smaller than $\frac{2\pi}{3}$, i.e., overall we bend at least 60° towards the inner side.*

Proof. Note that the argument for the inward directed bend at v_2 and v_4 in the proof of Lemma 7 was simply based on the number of extension neighbors. By increasing that number to 3, the lemma immediately follows.

We call this construction a corner connector. The corner connector contains a 5-cycle, however similar to a 4-cycle, it is impossible to place a disk inside such a cycle without creating wrong adjacencies through overlap.

Finally we want to state some measure for the height of a UDR of an augmented L_k

Lemma 9. *The height the smallest bounding rectangle of a UDR of an augmented ladder L_k is at least $2\sqrt{3} + 2 - \varepsilon''$, where ε'' is a very small constant, which is the height of the smallest bounding box of an optimal packing of three rows of unit disks minus ε'' .*

Proof. The distance between the extension neighbors and the outer disks of the ladder has been argued in the proof of Lemma 7. Recall that the disks of the outside vertices of the ladder with a single extension neighbor are almost completely covered by it. Let $d(v_k)$ be such a covered disk. Its adjacent disk $d(v'_k)$ on the inside of the ladder can therefore only overlap a very small amount with $d(v_k)$. Since $d(v'_k)$ is disjoint from $d(v_{k-1})$ and $d(v_{k+1})$, the extreme position (see Fig. 12d) results in the smallest overall height of the ladder, which is the height of the dense packing of three rows of unit disks, i.e., $2\sqrt{3} + 2$ minus the small amount ε'' which is attributed to the small possible overlap of $d(v'_k)$ and $d(v_k)$.

Now we have all necessities to describe the construction of the 7-stable approximations of a long thin rhombus (Lemma 1) and a regular hexagon (Lemma 2). Two ladders L_k and L'_k are placed opposite each other and connected on one end with three corner connectors as shown in Fig. 4. Note that the horizontal distance between c_0 and v_1 is four.

Lemma 1 (\star) . *For every positive integer k the outerplanar graph G_k^R in Fig. 4 is a 7-stable approximation of a rhombus of width $2k + 6$ and height $6\sqrt{3} + 2$.*

Proof. We can assume that $v_0 = (0, 0)$ and that $c_0 = (-2, 0)$. We define a point $l_0 = (2k + 4, 0)$ on the positive x -axis with.

We place a congruent copy of the rhombus, s.t., the long diagonal aligns with $\overline{c_0 l_0}$, and one corner point coincides with the leftmost point of c_0 , which is at $(-3, 0)$. At every point the upper and lower boundary of the rhombus has a vertical distance of $\delta \in [0, 3\sqrt{3} + 1]$ to $\overline{c_0 l_0}$. Due to Lemmas 7 and 8, the overall bend of L_k and L'_k has to be towards the inner side. In fact the position depicted in the Fig. 4a is the limit and would require an additional infinitesimal bend inwards to be valid. A consequence is that c_0 and any a_i , have a maximal vertical distance of $3\sqrt{3}$ and therefore any point on the boundary of any disk has at most a vertical distance of $3\sqrt{3} + 1 \approx 6.196 < 7$ to $\overline{c_0 l_0}$.

Clearly the UDRs of L_k and L'_k are completely overlap-free and therefore a tight packing as indicated in Fig. 4b is the narrowest possible configuration (including a small gap between the ladders).

Now consider, that the smallest rectangular bounding box of the disks of the of outer vertices v_1, \dots, v_k and v_{-1}, \dots, v_{-k} (as labeled in Fig. 4a) and their extension neighbors have a combined height of at least $3\sqrt{3} + 2$, which is the height of an optimal packing of four rows of unit disks. Therefore, at every point, there is part of the outline of G_k^R on or above, and on or below $c_0 l_0$ and

the distance of the boundary of the union of all disks and the boundary of the rhombus is at most the distance of the rhombus itself to $\overline{c_0 l_0}$, which as stated before, is $3\sqrt{3} + 1 < 7$.

Next we will create a 7-stable approximation G_k^H of a regular hexagon by tracing the outline of a hexagon with ladders and corner connectors as shown with the blue and the red disks in Fig. 5a. Every side of the hexagon is represented by a L_{k-3} . Let L_j^1, L_j^2 be two ladders, and let v_i^k and u_i^k be the i -th outer and inner vertices of L_j^k respectively. At a corner, where L_j^1 and L_j^2 meet, we connect u_j^1 and u_j^2 with an edge. Further, we connect the vertex v_c of the corner connector with v_j^1 and v_j^2 , thereby connecting the two ladders with a corner connector. The construction is depicted in Fig. 3b. Six ladders are connected in this fashion through the use of five corner connectors, leaving the first and the last ladder disconnected. This forms the outer hull of the hexagon, shown in Fig. 5a.

Since bends towards the outer side are impossible, we next need to control the possible deformation of a UDR of our construction towards the inner side. To achieve this, we add ladders to our construction on the inside of the hull, reminiscent of our construction of G_k^R . We chose the size of the hexagon, s.t., the inner area of a UDR of the hull admits the placement of $2m$ ladders ($m \in \mathbb{N}$ on the top and on the bottom, each) and that in a UDR, which is an optimal packing of disks, there is no space to add further disks in the gaps, without creating false adjacencies.

Lemma 2 (\star). *For every integer $k = 6n + 4, n \in \mathbb{N}$, the outerplanar graph G_k^H in Fig. 5a is a 7-stable approximation of a regular hexagon of side length $2k - 1$.*

Proof. By combining Lemmas 7 and 8, we conclude that a UDR of a such constructed outer hull does not exceed the boundary of a translated and/or rotated copy of the hexagon outlined as a dashed line in Fig. 5a, which has a side length of $2k - 1$.

Some movement towards the inside is possible. By moving all ladders on the inside in the top half down by a complete row, including the ladder tracing the upper horizontal edge of the hexagon, we again arrive at an optimal packing of pairwise disjoint ladders, which contribute (due to Lemma 9) at least their full height of $2\sqrt{3} + 2 - \varepsilon''$ (again ε'' is a very small constant value) to the height of any UDR of the construction and theoretically, there is space to fold the right outer arm inward as depicted in 13a. Even though the depicted folding of this outer arm into the optimal packing position is not possible, due to the construction, for increasingly long outer arms, we can get arbitrarily close to this packing. Therefore we analyze the (unreachable) worst case of the optimal packing, in which the farthest point from the boundary of the hexagon has a distance of $3\sqrt{3} + 1 + O(k) \cdot \varepsilon'' < 3\sqrt{3} + 1 < 7$, we conclude that no point on the boundary of the union of all disks in the UDR of a G_k^H has a larger distance than 7 to a point on the boundary of the green dashed hexagon.

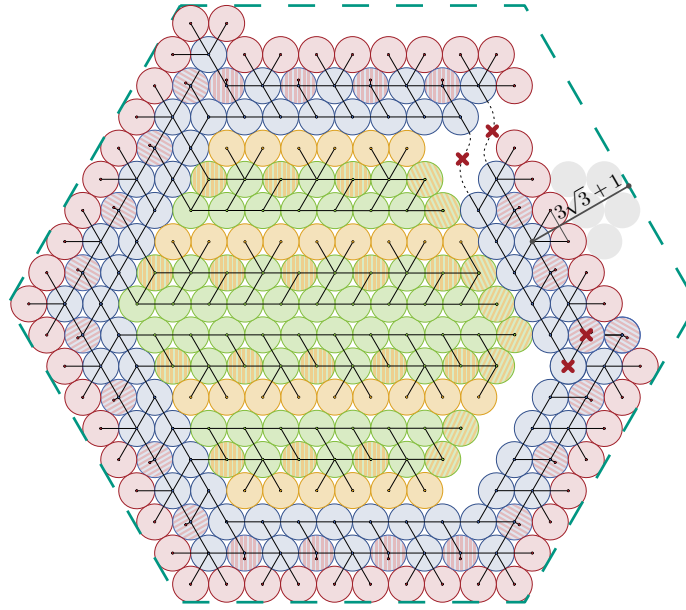
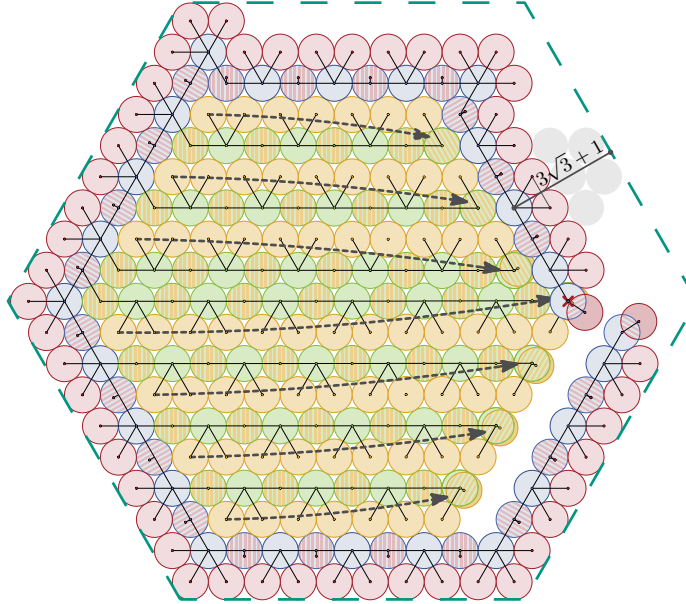
(a) Compact state of G_k^H (b) Compact state of T_k^H

Fig. 13: In the most compact position, the UDR of G_k^H and T_k^H can – similar to the rhombus – fold all inner arms to one side (here to the lower side), and theoretically, there is space to fold the outer arms inward as depicted. The UDR of the arms are however again pairwise overlap free and the largest reachable distance any point on the boundary of the union of disks can have from the approximated regular hexagon is $3\sqrt{3} + 1$.

A.5 Proof of Theorem 2

Theorem 2 (\star). *Recognizing unit disk graphs is NP-hard for embedded trees.*

Proof. By modifying the construction of the previous section, we can prove that given a tree T and an embedding $\mathcal{E}(T)$ it is NP-hard to decide if T admits a UDR \mathcal{D} , s.t., $\mathcal{E}_{\mathcal{D}}(T) = \mathcal{E}(T)$. In particular, we construct two graphs T_k^R , T_k^H , which are both trees and 7-stable approximations of a long thin rhombus and a regular hexagon respectively.

In the previous proof, we needed to construct ladders in a very specific way to force the placement of the disks of extension neighbors to one side. This was done by adding the inner vertices, which made the graphs outerplanar. Since in this setting the embedding is fixed, we can remove the inner vertices, which leaves the outer vertices and the extension neighbors. Observe that the leftover graph is a tree. The same holds for the corner connector.

Lemma 7 and Lemma 8 can be directly applied to this new construction, since no assumption was made about the placement of the inner vertices outside of their function of forcing the disks of the extension neighbors to be placed on the outside. This is now guaranteed by the embedding that is given as input.

To construct T_k^R , remove the inner vertices of a G_k^R . Now the space between the two arms is large enough to accommodate one of the arms folding in on itself. To prevent this, we add a third arm to the construction, as shown in Fig. 6a. Recall that the outer arms of the construction cannot bend farther outwards than to the horizontal position in Fig. 6a. Now again, no singular disk can be fit into the gap between the arms.

Next note that even without the inner vertices of the ladders, the three arms of a T_k^R must together always be at least as high as an optimal packing of six rows of disks, which results in a height of $5\sqrt{3} + 2$. Therefore, at any given horizontal point, some part of the boundary of the union of all disks in a UDR of T_k^R is either on or above $\overline{c_0 l_0}$. Since any point on the approximated rhombus is at most $3\sqrt{3} + 1 < 7$ away from this line, T_k^R is a 7-stable approximation of a long thin rhombus.

We perform a similar adaption of G_k^H to obtain T_k^H , a 7-stable approximation of a regular Hexagon. Analogously to T_k^R the outer hull, which traces the hexagon is the same as for G_k^H , with all inner vertices removed from the ladders. The relative placement of disks of extension neighbors to the outside is fixed, by the given embedding. Therefore we can always place a congruent translated and/or rotated copy of the hexagon we want to approximate over the UDR of the construction shown in Fig. 5b, s.t., the UDR is completely contained.

The exact placement of the inner ladder is slightly different as before. We still fill the inside in such a manner, that the space between all upper and lower inner ladders does not admit the placement of an additional disk in a UDR, if realized as an optimal packing (cf. Fig. 5b), however this requires an asymmetric construction, which places one additional ladder on one of the two sides, here to the bottom (similar to the construction of T_k^R). Movement to the inside can be analyzed with a similar approach as before, by considering the closest placement

to the inside of any of the arms, resulting in an optimal packing of the entire upper half of the construction, as seen in Fig. 13b. Again this unobtainable worst case scenario leads to a maximal distance of $3\sqrt{3} + 1 < 7$ between the outline of any UDR of T_k^H and the hexagon.

We therefore obtain again 5-stable approximations of a long thin rhombus and a hexagon and hardness follows in the same fashion as for Theorem 1.

B Omitted Details of Section 4

B.1 Proof of Lemma 3

Lemma 3 (\star). *If B_G contains two adjacent degree 5 vertices u, v , then it does not admit a unit disk intersection representation.*

Proof. Let u_1, u_2, x (resp. v_1, v_2, x') be the first, second and third neighbor of u (resp. v) in counterclockwise/clockwise order, respectively. We assume a placement of $d(u_1), d(u_2), d(v_1)$ and $d(v_2)$ as depicted in Fig. 14. Since x is adjacent to u and not adjacent to u_2 and v , the possible space of placing the center of $d(x)$ is restricted to a small open fan-shaped area (see Fig. 14c). A symmetric area exists for $d(x')$ as well. Moreover, all three pairs of points with a distance of at least two, namely Figs. 14d and 14f and a symmetric version of Fig. 14f, are on the boundaries of these areas. Therefore no such pair exists in the open fan-shaped areas. Note that a similar argument holds for the lower side and any rotation of $d(u_1), d(u_2), d(v_1)$ or $d(v_2)$ will decrease the area on one side. This completes the proof.

B.2 Correctness

If a caterpillar contains consecutive degree 5 vertices we reject it as it has no UDR. In any other case, the algorithm above can represent it in a way, s.t., at any point the angle between a backbone vertex and its left most-top and left-most bottom leaf is less than π . As long as this property holds, we can always add a new backbone vertex. Moreover, if the sequence is extended by a backbone vertex of at most degree 4, this property immediately holds again. If the sequence is extended by a backbone vertex of degree 5, a backbone vertex of degree at most 4 must follow. Once we place this degree 4 vertex appropriately, cf. Fig. 7b, then the property immediately holds again.

C Omitted Details of Section 5

Observation 1 (\star). *The number of possible placements of a backbone vertex v_i and its descendants is constant for a fixed position of v_i .*

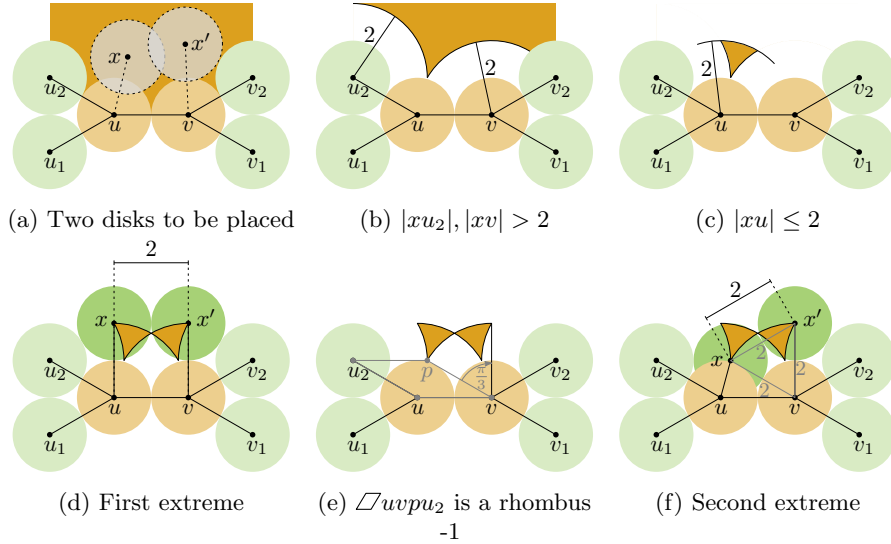


Fig. 14: Visualization of the proof steps of Lemma 3. The area highlighted in orange illustrates possible placements for the center of $d(x)$, which is progressively restricted by its adjacent and non-adjacent neighbors.

Proof. The vertex v can only be placed at one of three possible grid positions. For each position p at which v can be placed, every placement of v and its descendants corresponds to a subset of the constant size set $S(p)$, which yields again a constant number of placements.

Observation 2 (★). *For a fixed grid position, the number of backbone vertices of a strictly x -monotone weak UDC, who can occupy this position by themselves or with a descendant is constant. Moreover, the distance in graph between the first and the last such vertex is constant.*

Proof. Clearly the number of grid positions inside a circle of radius 2 are constant. Therefore only a constant number of previously placed backbone vertices could have possibly been placed at this grid position or placed one of their descendants on it. Since the weak UDC is strictly x -monotone, every backbone vertex must be placed to the right of the previous one. In particular that means that only a constant number of backbone vertices can have a distance smaller or equal to 2 in x direction to the grid position and moreover, the graph distance between the first and last such vertex has to be constant. Since every graph, which possible can occupy the grid position has to have an x -distance of less or equal to 2, this concludes the proof.

Observation 3 (★). *Let C be a sufficiently large constant, and let A, B be two weak UDC, whose last C backbone vertices have placed themselves and their descendants in such a manner, that the pattern of occupied grid positions and the*

placement of the last backbone vertex is equivalent up to translation and rotation. Then any extension graph C , which can be appended to A , s.t., the combined graph admits a weak UDC can also be appended to B , s.t., their combined graph admits a weak UDC and vice versa.

Proof. Let U be the weak UDC of A and C . Now we take the subpart of U induced by vertices of C . Assume w.l.o.g., that the disk of the first backbone vertex of C was placed one grid position to the right of the disk of the last backbone vertex of B . We now translate this part, s.t., the disk of the first backbone vertex of C is placed one grid position to the right of the last backbone vertex of B . Since B and A had the exact same set of already occupied grid positions, this is a valid weak UDC of B .

Lemma 4 (\star). *Using dynamic programming it can be checked in linear time if a lobster graph admits an x -monotone weak UDC on the triangular grid.*

Proof. The dynamic program starts at the first backbone vertex V_1 , which is w.l.o.g., placed at a fixed position and enumerates all possible placements of the descendants of v_1 . Due to Observation 1, this can be done in $O(1)$ time. Every single placement yields a pattern of occupied positions on the grid. Note that two placements, which yield the same occupation pattern and place v_1 at the same position relative to that pattern (up to translation and rotation) are indistinguishable, when considering the obstruction they pose for the rest of the weak UDC, due to Observation 3. We save all possible occupation patterns together with the position of the previously placed backbone vertex as a record. After processing the first backbone vertex, we therefore clearly have a constant number of records.

When the dynamic program continues on from the $(i-1)$ -th to the i -th backbone vertex v_i it needs to place the new backbone vertex at a specific position. Every such position p has a constant set of grid positions, which are at most at a grid distance of 2 to p . Note that these grid positions can be occupied by descendants of previous backbone vertices, however, due to Observation 2 these backbone vertices have at most a constant distance in the graph to v_i . Therefore the dynamic program only needs to remember the exact occupation pattern for a constant number of previously placed backbone vertices.

In particular this means, that for all possible occupation patterns (a constant number per backbone vertex) of all relevant previous backbone vertices (a constant number) we need to save all possible placements (a constant number per backbone vertex and occupation pattern). We call one such saved combination, together with the position of the previously placed backbone vertex, a *record* and such a record is clearly of constant size.

For every single record, we need to enumerate all possible placements of the descendants of v_i . Due to Observation 1, this is also a constant number. Finally we can check if the placement is valid for this record in constant time. For every record, we now save for every possible valid placement of v_i and its descendants only the information of the occupied grid positions for v_i and the required constant number of predecessors of the backbone. The crucial observation is that

we do not need to differentiate between two records, which are equivalent as defined in Observation 3. If we do consider records, whose last C backbone vertices induce the exact same pattern and whose last backbone vertex was placed at the exact same position (up to translation), then it is clear that only a constant number of unique records exist for a single backbone vertex. In particular, v_{i+1} starts only with a constant number of records to check. This results in only an overall constant time to process a single backbone vertex.

D Computer Assisted Proof of Lemma 5

Here we aim to provide a detailed overview of our computer assisted approach of the induction step for the proof of Lemma 5. Recall that the induction hypothesis is as follows. Any lobster graph G , with a backbone of length k admits a strictly x -monotone weak UDC. In the induction step we need to prove that any extension to a lobster graph G' with a backbone of length $k+1$ also admits an x -monotone weak UDC. Let v_1, \dots, v_{k+1} be the vertices of $B_{G'}$. Note that v_{k+1} needs to be placed, s.t., it is in contact with v_k and, in a strictly x -monotone weak UDC, v_{k+1} can be placed at one of three possible grid positions p_1, p_2, p_3 , while in a weak UDC it can be placed at one of six possible grid positions p_1, \dots, p_6 (at least one of which will already be occupied by v_k). If we can find an instance of a graph G' , s.t., v_{k+1} is forced to be placed at one of the positions p_4, p_5, p_6 in order to realize a weak UDC of G' , we know that the Theorem would be false. The crucial observation is that we can enumerate for a given graph G all possible extensions G' , since the maximum degree of every vertex is naturally bounded by six. Moreover the exact structure of G is not relevant, when investigating if G' admits a weak UDC. But rather, we want to know to what extent the already placed disks of G can interfere with a placement of disks belonging to v_{k+1} and its neighbors.

D.1 Enumerating All Combinations of Free Grid Positions

Note that the set of grid positions, which can be used to place v_{k+1} or one of its neighbors is a constant size set of 29 positions, see Fig. 15a.

We assume w.l.o.g. that v_k was placed at grid position -1 . The positions we need to consider, when looking at obstructions is a smaller set than the full 29, as positions 21, \dots , 27 can not possibly be occupied, since they have a minimal grid distance of three to any possible previous backbone vertex position (Note that we denote the grid distance between two neighboring grid positions as one, even though the actual distance has to be two to accommodate the unit disks). Further we can assume -1 to be blocked as v_k is placed at this position

Next we can assume that the grid position -1 has to be connected to the left hand side of the area outlined in red in see Fig. 15a, as there must be at the very least an incoming path of backbone vertices. Every such x -monotone path on the grid starting at any point to the left of $-$ on the boundary of the red region and ending at -1 has a maximum length of three. Note that our base

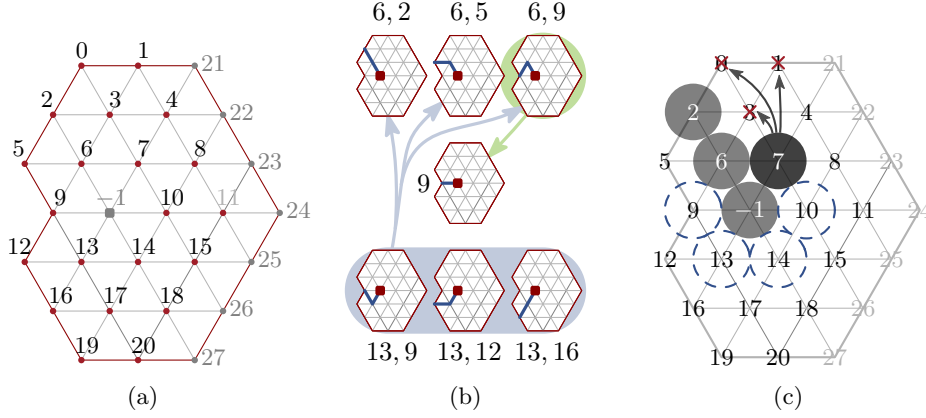


Fig. 15: (a) A constant size set of grid positions, which could be occupied by v_{k+1} or one of its neighbors for a fixed position of v_k (at -1) and a possible placement of v_{k+1} at either 7, 10 or 14. Positions, which are necessarily free (assuming an already x -monotone placement of v_1 up to v_k) are 21, \dots , 27. (b) All cases, how the previous backbone could be connected to the position of v_k . The numbers indicate the occupied positions of the previous backbone vertices in each case. The top right case is covered, because the center case is a subset of it. The bottom three cases are covered by symmetry.

cases cover all backbone lengths up to a length of three. Various possibilities exist for such a path, however we only need to consider three, see Fig. 15b. The top right case is covered, because it is indistinguishable from the center case, when a single neighbor of either v_k or v_{k-1} is placed at position 6. The bottom three cases are simply symmetric to the top three cases.

This now leaves us with two cases with a set of 19 possibly occupied grid positions and one with 20. From here on out we assume that we represent these grid positions as three lists of boolean variables L_C , $C \in \{\{6, 2\}, \{6, 5\}, \{9\}\}$ of length 21, where $L_c[i]$ ($\neg L_c[i]$) means that the position is (not) occupied. Clearly some of these positions are fixed to be true, e.g., $c \in C \implies L_C[c]$, i.e., the grid positions, which are occupied by disks of the previous backbone vertices are guaranteed to be blocked. Moreover, some of the positions are also guaranteed to be not occupied. For example the grid positions 19 and 20 do not have any path to either -1 , 2, 6, or any possible position of a previous backbone disk - recall that the realization is x -monotone up to v_k - of grid distance 2 or shorter and can therefore not be occupied by a previously placed disk. All possible combinations of the values in these lists, still leaves us with two times 2^{19} plus 2^{20} (since $L_{\{6,2\}}$ and $L_{\{6,5\}}$ have two blocked spots and $L_{\{9\}}$ has one) cases.

We can reduce the number even further when considering the implication of one true value on all other values in a list L_C . For this we first set every singular entry in a list to true and consider its implications. One example is shown in Fig. 15c, where we consider the implications of setting $L_{\{6,2\}}[7]$. Since

7 is occupied, the next backbone disk can only be placed at positions 9, 10, 13 or 14. Note that positions 0, 1 and 3 do not have a free path (that is a sequence of free grid position), s.t., the start and end point of this path have grid distance two to either one of these positions. Therefore, They are unusable to any descendent of v_{k+1} in a weak UDC. We can consider them occupied. This implication can be formulated as

$$L_{\{6,2\}}[7] \implies L_{\{6,2\}}[0] \wedge L_{\{6,2\}}[1] \wedge L_{\{6,2\}}[3]$$

We can manually consider every single position in the grid and their implications on all other positions in each of the three scenarios. All such implications are visualized as an implication matrix in Figs. 16a, 17a and 18a.

We further considered the implications of some sets of grid positions, e.g., $L_{\{6,2\}}[7] \wedge L_{\{6,2\}}[10] \implies L_{\{6,2\}}[4]$, i.e., in the $L_{\{6,2\}}$ setting, if both 7 and 10 are occupied, 4 is unreachable and can therefore be considered occupied. All such implications are again visualized in an implication matrix in Figs. 16b, 17b and 18b.

We then generate all possible combinations of Boolean variables for the three lists $L_{\{6,2\}}$, $L_{\{6,5\}}$ and $L_{\{9\}}$, but omit any combination, which contradicts any of the implications, we have identified, e.g., if any combination has

$$L_{\{6,2\}}[7] \wedge \neg L_{\{6,2\}}[0]$$

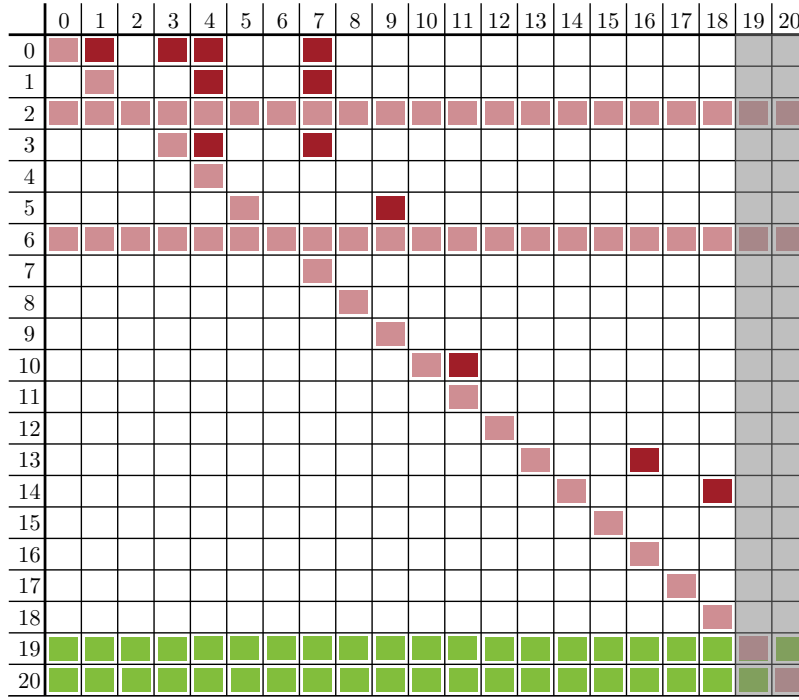
then we can omit it and similar for all other implications.

D.2 Enumerating all possible Extensions of G to G'

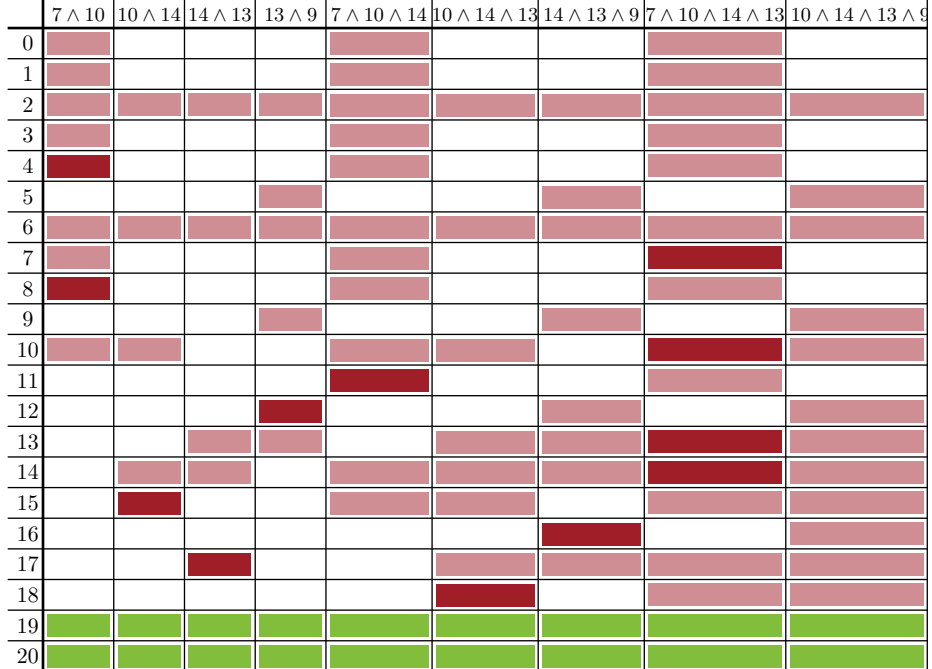
The next crucial observation is that the number of the neighbors of v_{k+1} and the number of their neighbors is bounded by 5, i.e., $v_k k + 1$ can have at most 5 neighbors (excluding v_k), which can have at most 5 neighbors themselves (excluding v_{k+1}). Again we represent v_{k+1} as a sorted list L_v of length equal to the number of neighbors (excluding v_k), s.t., for every neighbor v_n of v_{k+1} , there is an i , s.t., $L_v[i]$ is equal to the number of neighbors of v_n (excluding v_{k+1}). For example, the first backbone vertex of Fig. 1c, would be represented as $[3, 2, 1]$.

Now it is clear that we can employ again an exhaustive enumeration to construct every sorted list of length 5 or lower, with all possible combination of values between 0 and 5. We can however again identify some exclusion criteria, based on structures, which make a graph unrealizable outright. These criteria are:

- If the total number of vertices is larger than the not occupied entries in L_c , the graph is not realizable
- Depending on the number of neighbors (excluding v_{k+1}) we can identify, how many grid positions at grid distance 1 to the placement of v_{k+1} , a single neighbor will occupy
 - If $L_v[i]$ equals 5, it will occupy at least 3 such spaces, (2 additionally)
 - If $L_v[i]$ equals 4, it will occupy at least 2 such spaces (1 additionally)

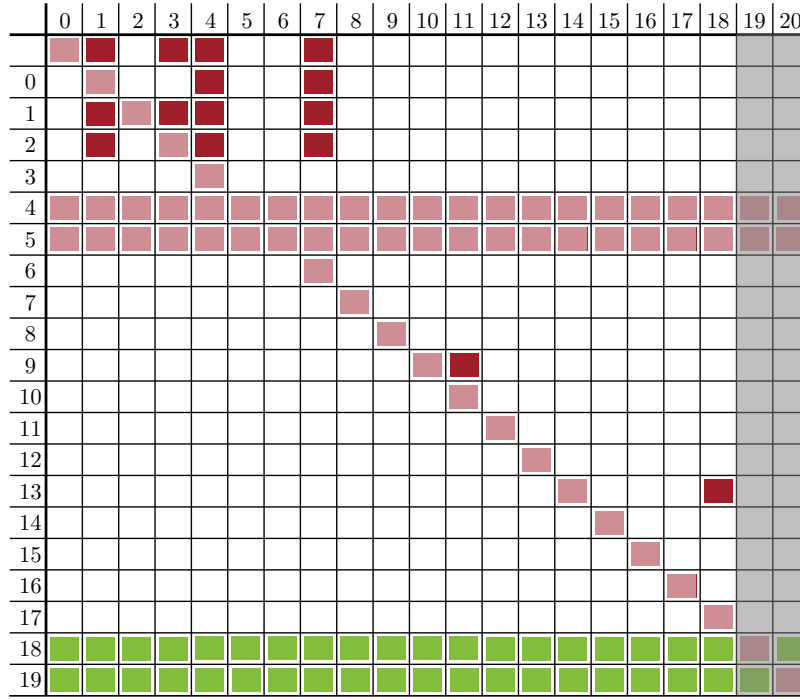


(a) Implications of singular grid positions



(b) Implications of sets of grid positions

Fig. 16: Implications of singular grid positions being occupied on all other grid positions in $L_{\{6,2\}}$. Red blocks indicate, the column number implies the row number. Light red blocks indicate a trivial or previously determined implication. Green blocks indicate guaranteed free positions. Grey overlay indicates that the implication of these columns was not considered (as they are free).

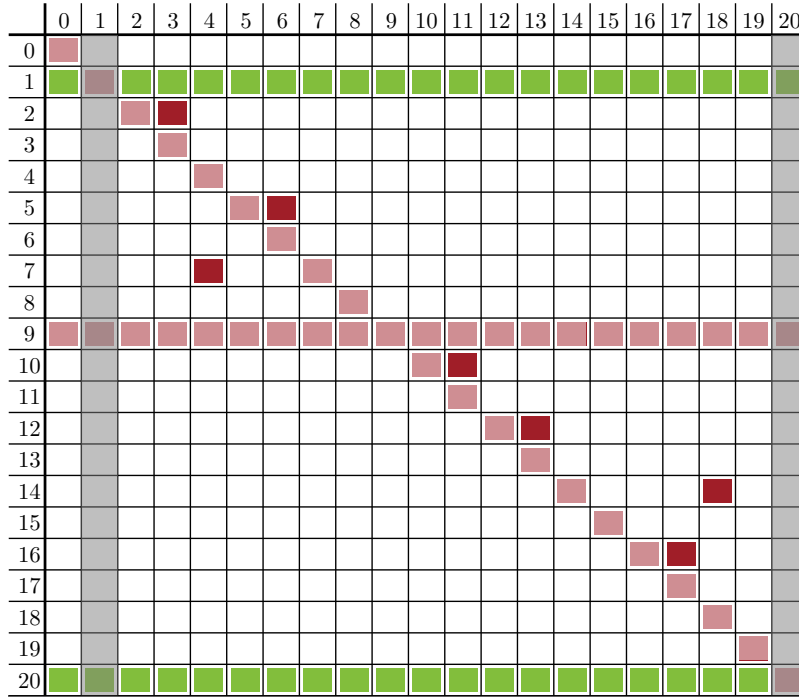


(a) Implications of singular grid positions

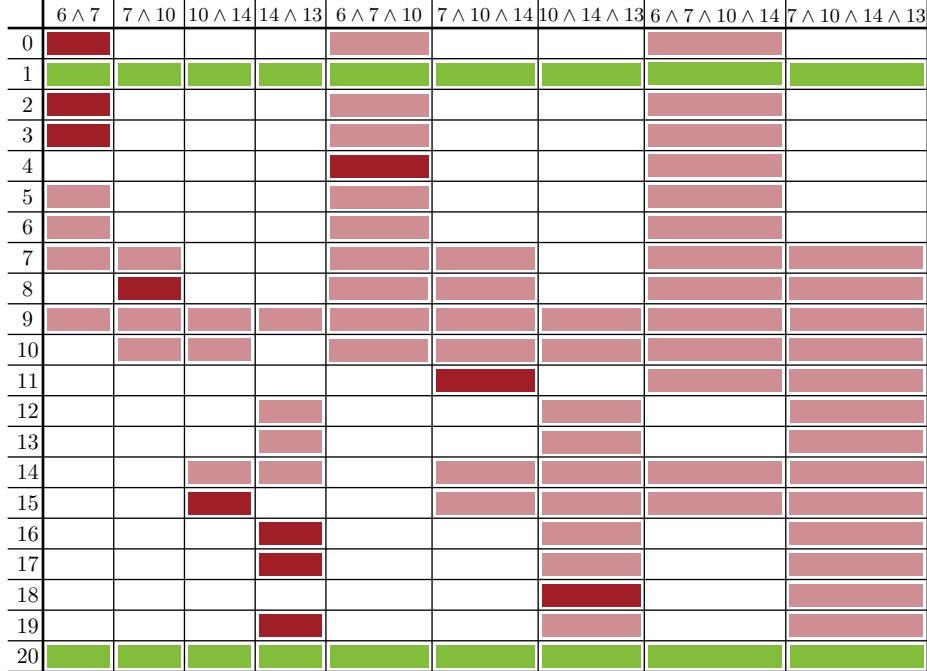


(b) Implications of sets of grid positions

Fig. 17: Implications of singular grid positions being occupied on all other grid positions in $L_{\{6,5\}}$. Red blocks indicate, the column number implies the row number. Light red blocks indicate a trivial or previously determined implication. Green blocks indicate guaranteed free positions. Grey overlay indicates that the implication of these columns was not considered (as they are free).



(a) Implications of singular grid positions



(b) Implications of sets of grid positions

Fig. 18: Implications of singular grid positions being occupied on all other grid positions in $L_{\{9\}}$. Red blocks indicate, the column number implies the row number. Light red blocks indicate a trivial or previously determined implication. Green blocks indicate guaranteed free positions. Grey overlay indicates that the implication of these columns was not considered (as they are free).

- If there exists i, i', i'', i''' , s.t., $L_v[i], L_v[i'], L_v[i'']$ are equal or greater than 3 and $L_v[i''']$ is equal or greater than 2, these neighbors will together occupy at least 5 such spaces (1 additionally)

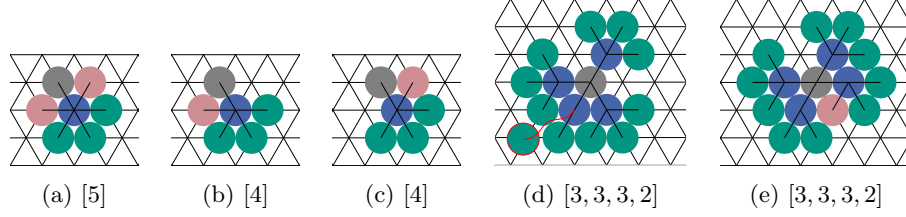


Fig. 19: Additionally occupied grid positions at grid distance 1 from the position of v_{k+1} (grey). A descendant, which is non-adjacent to v_{k+1} , but occupies a grid position at grid distance 1 to v_{k+1} is colored in light red. The realization in (d) is not valid. The subcaptions are according to the list notation of the neighbors as used in the text.

If any of the first two criteria applies or the number of neighbors of v_{k+1} plus the number of additionally occupied grid positions (indicated in parenthesis above) is greater than the number of free spaces at grid distance 1 to the chosen position of v_{k+1} , we can disregard this sorted list.

With these tools, we can now generate the set of instances $I = (\Gamma \times \Theta) \setminus \Xi$, where Ξ is any combination of an element $\gamma \in \Gamma$ and $\theta \in \Theta$, s.t., either γ or θ or the combination of both could be excluded based on the criteria outlined above. The size of I is $|I| = 7017913$.

D.3 Enumerating All Possible Realizations in a Given Setting

Finally we use an exhaustive enumeration of possible placement of the descendants of v_{k+1} , for each of the three or six possible placements of v_{k+1} to generate Δ_3 and Δ_6 . For this we consider a fixed position of v_{k+1} . Then we consider every possible placement of its neighbors on the grid positions at grid distance 1 to v_{k+1} . If no such placement exists, the setting is not realizable. Next for a neighbor v_n of v_{k+1} we consider all placements of its neighbors (excluding v_{k+1}) at the still free grid positions. If this does not exist for any v_n , the setting is not realizable. Now we have multiple sets of possible realizations of the neighbors of every v_n . We finally consider every combination of choosing one element out of each of these sets, s.t., no two disks occupy the same grid positions. If no such combination exists, the setting is not realizable. Otherwise the set of all combinations is a complete enumeration of all realizations of v_{k+1} and all of its descendants.